Development of Cu(II) Doped Boehmite Based Multifunctional Sensor for Detection, Removal of Cr(VI) from Wastewater and Conversion into an Energy Harvesting Material

Shubham Roy[1], Souravi Bardhan[1], Dipak Kr. Chanda[2], Saheli Ghosh[1], Dhananjoy Mondal[1], Jhilik Roy[3], Sukhen Das[1*]

[1]Department of Physics, Jadavpur University, Kolkata-700032, India

[2]Advanced Materials and Mechanical Characterization Division, CSIR-Central Glass and Ceramics Research Institute, Kolkata- 700032, India

[3]Department of Physics, Techno India University, Kolkata-700091

Supporting Information

*Corresponding Author:

Sukhen Das

Address: Jadavpur University, Raja S.C.Mullick Road, Kolkata- 700032

Email id: sdasphysics@gmail.com

Contact No.: +91 9433091337

S1. Characterizations of the synthesized MFNS

Crystallinity and microstructural parameters of the sample (CBH) have been investigated by employing X-ray powder diffraction method. Figure S1(a) shows the XRD pattern of synthesized nanostructure of Cu-doped boehmite which has been recorded by using a D8, BRUKER AXS, Powder X-Ray Diffractometer, using Cu-Kα radiation (λ = 1.5405 Å) in the varying range of 2θ (10º to 70º). The scan speed was set at 0.02 with an accelerating voltage of 35 kV and 35 mA. Furthermore, the XRD pattern of the sample has been refined by using Rietveld based software package MAUD (version: 2.8) software and the lattice parameters and other crystallographic parameters have been estimated. The X-Ray diffractogram was superimposed with the corresponding miller indices (Joint Committee on Powder Diffraction Standards card no. 21-1307), which shows well-matched peak positions indicating high purity and microstructural properties (Table. S1, S2) simultaneously. VESTA v3.4.3 (Visualization for Electronic and Structural Analysis) computing platform enables us to compute the bonding networks (Table S3 and Table S4) and it also provides us with the clear microstructural representation of the copper doped boehmite sample (Figure S1(b), Table S2) [1].

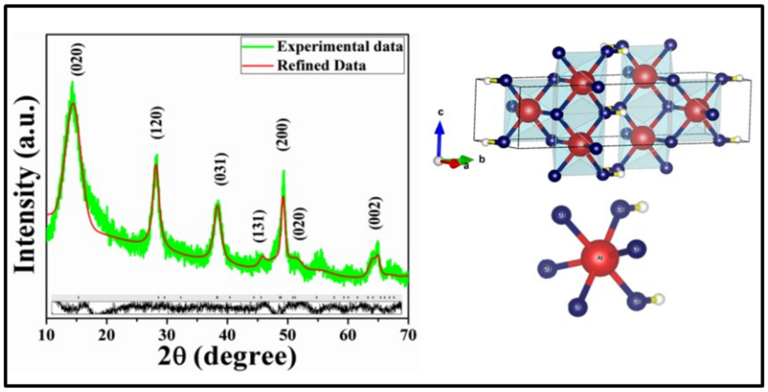

Figure S1. XRD pattern and corresponding microstructural diagram of CBH

Rietveld refinement shows that the synthesized powder is in nano-dimension with a crystallite diameter of 19.488 nm. The results obtained after the final cycle of refinement regarding structural, microstructural and reliability parameters of the samples are provided in Table S2. A slight shifting of diffraction maxima towards the higher diffraction angle with respect to the JCPDS card: 21-1307 is caused due to the internal homogeneous lattice stress (microstrain value is 0.0045403317) developed inside the lattice structure that enforced by copper doping [2].

Table. S1 Structure parameters of CBH obtained from Rietveld refinement.

Atom	x	y	z	B_{iso}	Occupancy
Al	0.250000	-0.317730	0	1	1
O1	0.250000	0.289613	0	1	1
O2	0.250000	0.080952	0	1	1
H	0.249680	0.002923	0	0.5	0.04

Table. S2 Structural and microstructural parameters of the CBH obtained from Rietveld refinement of XRD diffractograms.

Parameters	Values
a	3.7005575± 0.0035226033 Å
b	12.196083 ± 0.039433066 Å
c	2.8705513 ± 0.0018715553 Å
size	194.88666 ± 5.799716 Å
strain	0.0045403317 ± 5.0732365x10^{-4}
χ^2	1.723
Cell volume	129.5546 $Å^3$

Table. S3 Variation of the bond lengths of CBH.

Nature of the bond	CBH(Å)
Al-O (O_1)	1.88179
Al-OH (O_2)	1.89392

Table. S4 Variation of the bond angles of CBH.

Angle between	CBH(degree)
OH-Al-O	96.8283
OH-Al-OH	98.5472
O-Al-O	82.9460

In order to get an overview of the bonding network formation inside the orthorhombic cells of boehmite, FTIR spectroscopy has been performed by using an FTIR-8400S infrared spectrophotometer and depicted in Figure S1(c). The spectrum shows no alteration from pure boehmite which indicates successful incorporation of copper ions inside the boehmite orthorhombic phase. The characteristic part of the spectrum confirms the purity of the nanostructure that has been matched using the AlO_6 vibration modes (480, 617 and 747 cm^{-1}) [3]. Symmetric and asymmetric modes of Al-O-H vibration have been confirmed with the help of two different bands located at 1069 and 1158 cm^{-1} respectively [4]. Two other vibrational bands located at 3095 and 3305 cm^{-1} corroborates to symmetric and asymmetric O-H vibrations respectively [5]. Additionally, the surface adsorbed moisture can be predicted using a 1634 cm^{-1} band [6]. Thus, our FTIR analysis supports the XRD data quite well.

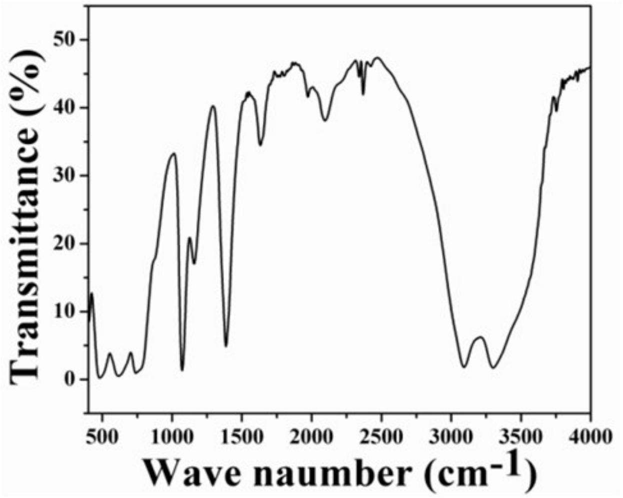

Figure S2. FTIR spectra of the CBH sample

Morphological investigation of the as-synthesized nanostructure has been made by using scanning electron microscopy [7]. The powder samples were ground in an agate mortar and directly mounted on the carbon-coated mesh followed by a sputter coating of platinum. SEM micrograph (Figure S1(d)) shows a combination of cubic and spherical nanoparticles. Some nano-flakes have also been observed which might be caused due to further agglomeration of spherical/ cubic particles. The mean particle size is found to be ~21.2 nm as the SEM micrograph suggests.

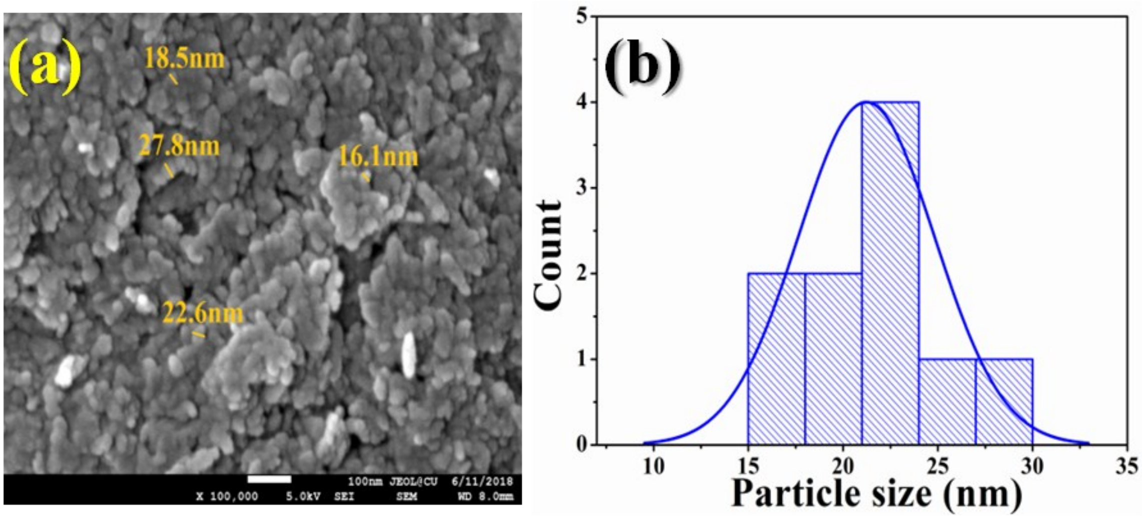

Figure S3. (a) SEM micrograph of CBH and (b) corresponding particle size distribution from SEM data

These nanostructures are further characterized using a transmission electron microscope to estimate the particle size and surface porosity (Figure S1(e)) [8]. A Jeol 2000 FX transmission electron microscope was employed for this purpose. A small amount of nano-powder was dissolved in acetone and then drop cast on a carbon-coated copper mesh to obtain TEM microscopy results. The TEM image of the sample shows an admixture of cubic and rectangular porous structures with an average particle dimension of 20 nm which agrees well with our SEM micrograph.

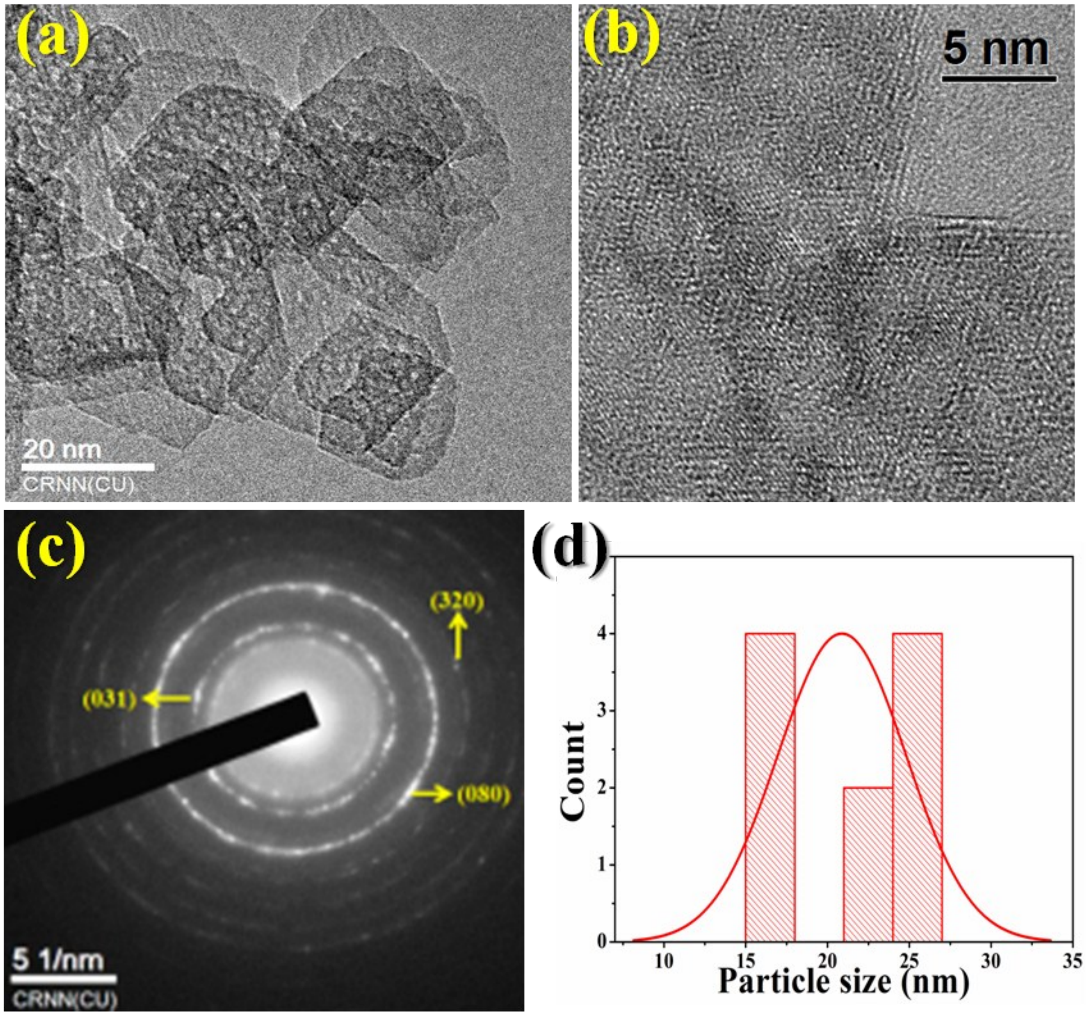

Figure S4. (a) TEM and (b) HR-TEM images of the synthesized CBH nanostructure, (c) corresponding SAED pattern and (d) particle size distribution data from TEM

Determination of the mean pore diameter of this ‘sponge-like’ porous sample along with the surface area is quite an important task [9]. Thus, the measurement is accomplished by using standard Brunauer-Emmett-Teller (BET) and Barrer-Joyner-Halenda (BJH) method by employing a Surface Area Analyzer (Quanta-chrome Instruments, USA) [10]. The adsorption-desorption hysteresis loop was estimated by using nitrogen gas. Figure S1(f) shows that the adsorbed and desorbed volumes of nitrogen are almost similar to each other which results in a type IV isotherm suggesting the presence of mesopores in our sample [11]. CBH has a mean pore diameter of 3.913 nm (Table. S5) which makes it a promising adsorbent material.

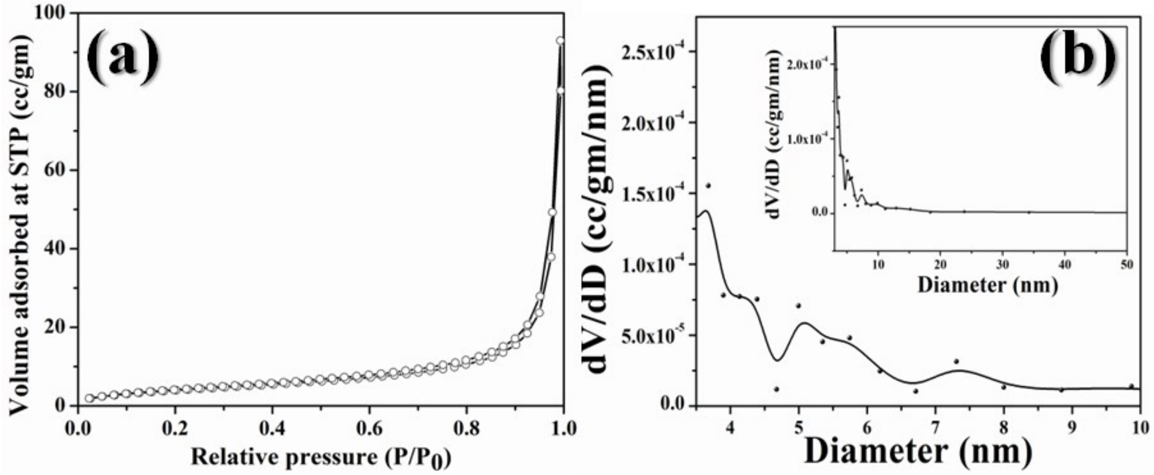

Figure S5. (a) N_2 adsorption/desorption isotherm of CBH; (b) corresponding pore size distribution data of CBH

Table. S5 Estimated BET surface area, pore radius and pore volume of the Cu-doped boehmite nanostructures.

Sample name	Surface area (m^2/g)	Pore size (nm)	Pore volume (cc/g)
CBH	15.297	3.913	0.213

Table. S6: Calculated fluorescence lifetime values from Fig.S1 with the increasing concentration of Cr (VI) ion.

Sample name	Cr(VI) ion concentration (μM)	Lifetime value (nS)
CBH	0	4.728995
CBH	50	4.123477
CBH	100	0.811854

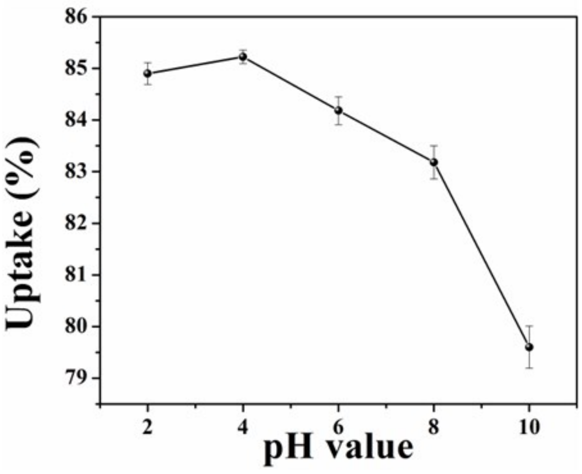

Figure S6. pH dependent adsorption uptake study for CBH

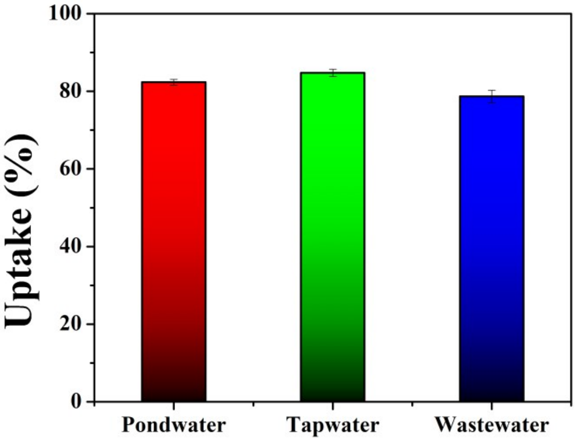

Figure S7. Estimation of sorption uptake of hexavalent chromium on CBH in presence of other disturbing ions

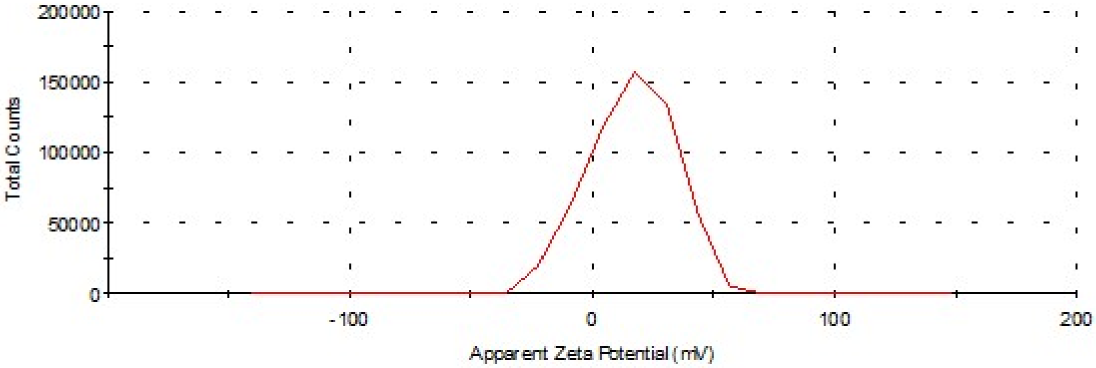

Figure S8. Surface charge (Zeta potential) study of CBH

Table. S7: Performance comparisons between selected fluorescent sensors for Cr(VI).

Material	Quenching constant (K_{SV}, M^{-1})	Detection limits (μM)	Waste to wealth conversion	Ref
$[Zn(btz)]_n$	4.23×10^3	2	NM	Cao et al. 2016
$[Zn_2(ttz)H_2O]_n$	2.19×10^3	20	NM	Cao et al. 2016
$[Eu(Hpzbc)_2(NO_3)]\cdot H_2O$	NM	22	NM	Li et al. 2016
$[Zn(2\text{-}NH_2bdc)(bibp)]_n$	6.55×10^6	NM	NM	Wen et al. 2015
Eu(III)@MIL-121	4.34×10^3	0.054	NM	Hao et al. 2016
Zn-MOF	7.59×10^3	3.9	NM	Lv et al. 2016
Nu-1000	1.34×10^4	1.8	NM	Lin et al. 2017
GBH1	0.0966×10^6	10.5	NM	Roy et al. 2019
CBH	**$0.163x10^6$**	**6.24**	**Energy harvesting**	**This work**

NM = not mentioned

Table. S8: Performance comparisons between selected Cr(VI) adsorbents

Material	Adsorption type	Maximum adsorption capacity (mg/gm)	Waste to wealth conversion	Ref
Nu-1000	Langmuir	q_m= 75	NM	. Lin et al. 2017
GBH1	Freundlich	NM	NM	Roy et al. 2019
L.sajor-caju	Langmuir	q_m= 6.3	NM	Arica and Bayramoglu 2005
Rice husks	Langmuir	q_m= 0.6	NM	Sumathi and Naidu 2005
Almond shell	Langmuir	q_m= 2.4	NM	Pehlivan and Altun 2008
Oak pine	Langmuir	q_m= 0.47	NM	Park et al. 2008
AGHP	Langmuir	q_m= 10.123	NM	Nasseh et al. 2017
Coal	Langmuir	q_m= 6.78	NM	Gao et al. 2008
CBH	**Freundlich**	**K_F= 1.564; n= 0.683 (Freundlich)** **q_m= 113.12 (Langmuir)**	**Energy harvesting**	**This work**

NM = not mentioned

References

1 A. Serafini, L. Lutterotti, S. Gross and S. Gialanella, *Powder Diffraction,* 2017, **32,** S63-S68.

2 S. Das, S. Das, A. Roychowdhury, D. Das and S. Sutradhar, *Journal of Alloys and Compounds,* 2017, **708***,* 231-246.

3 A. Zirehpour, A. Rahimpour, F. Seyedpour and M. Jahanshahi, *Desalination,* 2015, **371,** 46-57.

4 W. Brostow and T. Datashvili, *Chemistry and Chemical Technology*, 2008, **2,** 27-32.

5 A. Dandapat and G. De, *Journal of Materials Chemistry* 2010*,* **20***,* 3890-3894.

6 J. Zhang, S. Liu, J. Lin, H. Song, J. Luo, E. Elssfah, E. Ammar, Y. Huang, X. Ding and J. Gao, *The Journal of Physical Chemistry B,* 2006, **110,** 14249-14252.

7 K. Yoshimatsu, K. Reimhult, A. Krozer, K. Mosbach, K. Sode and L. Ye, *Analytica chimica acta,* 2007, **584,** 112-121.

8 S. Bardhan, S. Roy, D. K. Chanda, S. Das, K. Pal, A. Chakraborty, R. Basu and S. Das, *Crystal Growth and Design,* 2019.

9 D. K. Chanda, P. S. Das, A. Samanta, A. Dey, A. K. Mandal, K. D. Gupta, T. Maity and A. K. Mukhopadhyay, *Ceramics International,* 2014, **40***,* 11411-11417.

10 D. K. Chanda, A. Samanta, A. Dey, P. S. Das and A. K. Mukhopadhyay, *Journal of materials science,* 2017, **52,** 4910-4922.

11 J. Choi, K. S. Yoo, S. D. Kim, H. K. Park, C. W. Nam and J. Kim, *Journal of industrial and engineering chemistry,* 2017, **56,** 151-156.